PASJ: Publ. Astron. Soc. Japan **56**, 633–643, 2004 August 25
© 2004. Astronomical Society of Japan.

H I Jet G40−15 from a Rotating Cloud in the 4-kpc Molecular Ring: Magnetized Outflow and Formation of a Dense Star Cluster

Yoshiaki SOFUE
Institute of Astronomy, The University of Tokyo, Mitaka, Tokyo 181-0015
sofue@ioa.s.u-tokyo.ac.jp
Takahiro KUDOH
Department of Physics and Astronomy, University of Western Ontario, London, Ontario N6A 3K7, Canada
Akiko KAWAMURA
Institute of Space and Astronautic Science, Japan Aerospace Exploration Agency, Sagamihara, Kanagawa 229-8510
Kazunari SHIBATA
Kwasan Observatory, Kyoto University, Yamashina, Kyoto 607-8471
and
Mitsuaki FUJIMOTO
Department of Astrophysics, Nagoya University, Nagoya 464-8602

(Received 2004 March 4; accepted 2004 June 1)

Abstract

A giant H I spur centered on $(l, b) = (40°, -15°)$, (G40−15) emanates from G30−00 toward negative high latitude. The spur is known as the Smith cloud and as a high-velocity cloud HVC 40−15+100, while we call it H I jet G40−15. The radial velocity ranges from 80 to 120 km s^{-1} with the center velocity at ~ 100 km s^{-1}. Both the kinematical and positional coordinates are coincident with those of the tangential point of the 4-kpc molecular ring of the Galaxy. We interpret this spur as being a magnetized H I jet emanating from the 4-kpc molecular ring of the galactic disk. The kinematical distance is estimated to be 6.9 kpc from the Sun, and the jet's top (G50−26) is −3.4 kpc high from the galactic plane. The whole extent is 4.4 kpc in length and 300 pc in width. The total H I mass is $\sim 3 \times 10^5\, M_\odot$, and the energy to lift the mass from the galactic plane is $\sim 10^{52}$ erg. We propose an acceleration mechanism of such an extremely high-altitude coherent H I structure by a twisting magnetic jet associated with a collapsing molecular cloud in the galactic disk. We suggest a scenario for the formation of a dense star cluster, such as a globular cluster, from a collapsing cloud core with a twisting magnetic outflow.

Key words: galactic shock — Galaxy: H I — Galaxy: spurs — magnetic jets — molecular clouds — star clusters: formation

1. Introduction

Vertical gaseous spurs emerging from galactic disks are often observed in tilted spiral galaxies as out-of-plane vertical filaments, which provide information about the disk–halo interface and magnetism. Vertical ejections are evidence that the galactic disk is "boiling and steaming", possibly due to magneto-hydrodynamical (MHD) instabilities and/or ejections, as discussed for the starburst galaxy NGC 253 (Sofue et al. 1994).

The Milky Way is unique for its proximity as well as for the perfect edge-on orientation that reveals various vertical features emanating from the galactic plane. Radio spurs extending from the galactic plane are thought to be the result of inflation of gas, either due to explosive events in the disk, or magnetic inflation from galactic-shocked spiral arms (Sofue 1976). Radio spurs in the tangential directions of spiral arms are associated with H I spurs, indicating that they contain lifted neutral gas (Sofue, Tosa 1974). Wide field 21-cm line surveys exhibit numerous H I filaments and shell features, which are mostly out-of plane structures (Heiles 1996). The Leiden All-Sky H I survey with the Dwingeloo 25 m telescope (Hartman, Burton 1997) has revealed numerous out-of-plane H I features. Vertically extended H I features are present almost everywhere in the Galaxy with their roots in the galactic gas disk. Although their apparent morphology has been discussed extensively in the literature, a more quantitative description of the vertical structures, such as the energetics and dynamics, has been desired for understanding the origin and physics of the spurs.

In this paper, we consider a prominent H I spur, which is centered on G40−15 with a radial velocity of 100 km s^{-1}, apparently emanating from the 4-kpc molecular ring at G30−00 toward negative latitudes; we call it H I jet G40−15. The feature readily shows up clearly in the Leiden H I survey (Hartmann, Burton 1997). This H I jet has been known as the "Smith cloud" (Smith 1963). This feature is also named HVC 40−15+100 in their high-velocity cloud (HVC) catalogue of Wakker and van Woerden (1991). Bland-Hawthorn et al. (1998) have studied optical properties of this cloud in detail, assuming it to be an HVC out of the Milky Way, and discussed a possible association with the Sagittarius dwarf galaxy. In these studies, this H I feature is thought to be one of many high-velocity clouds surrounding the Galaxy, located far beyond the galactic disk.

On the other hand, Wakker and van Woerden (1991) have also suggested an alternative distance, if the cloud is assumed

to be associated with the galactic disk, and estimated the distance to be 6.5 kpc. They also estimated its mass to be $2.4 \times 10^5\,M_\odot$ from the H I intensity and distance. Thus, the distance ambiguity leaves both interpretations possible: either a high-velocity cloud, whose distance is unknown, but on the order of tens of kpc with mass and extent comparable to those of a dwarf galaxy, or a galactic spur associated with the 4 kpc molecular ring.

In this paper, we adopt the latter interpretation, that G40−15 is a galactic object associated with the 4-kpc molecular ring. From its coherent straight shape, we consider it to be a magnetic structure, and try to interpret the G40−15 H I spur to be a twisting magnetic jet from a collapsing magnetized molecular cloud in the dense molecular arm. In order to show that acceleration of a twisting magnetic jet from the galactic disk indeed occurs, we performed a simulation of an MHD jet from a magnetized collapsing cloud.

2. H I Jet G40−15

In order to investigate the kinematics and energetics of the H I jet G40−15, we used the Leiden all-sky H I survey data from Hartmann and Burton (1997), which provided us with a FITS formatted data cube of H I-line intensity at grid intervals of 0.°5 in the galactic coordinates and a velocity interval of $1.03\,\mathrm{km\,s^{-1}}$ in the LSR velocity. Figure 1 shows an H I intensity map of the whole sky integrated over $10\,\mathrm{km\,s^{-1}}$ around $90\,\mathrm{km\,s^{-1}}$. Figure 2 shows channel maps integrated every $5\,\mathrm{km\,s^{-1}}$ interval at $V_{\rm LSR} = 65$ to $125\,\mathrm{km\,s^{-1}}$ for the galactic first quadrant at $l = 20°$ to $55°$, $b = -30°$ to $+30°$. Figure 3 is the integrated H I intensity between 80 and $120\,\mathrm{km\,s^{-1}}$, and shows a close up in a contour map form. The prominent H I jet G40−15 is found as a bright H I ridge emanating from G30−00, extending to G50−26 with the maximum intensity position at around G40−15.

The angle between the H I jet's axis and the galactic plane is 52°, significantly leaning toward the outer Galaxy. The jet is lopsided with respect to the galactic plane, although a broad, but weak, counter jet may be recognized at around G38+10. Figure 3 shows that the jet bifurcates into two ridges at its thickest part around G42−17. Another narrower spur emerges from G32−00, which crosses H I jet G40−15 at G35−10 toward the opposite side, as if it winds around the major jet, and runs parallel to the main ridge.

From the mean recession velocity of $V_{\rm LSR} = 100\,\mathrm{km\,s^{-1}}$, the kinematical distance from the Sun is estimated to be 6.9 kpc by using the rotation curve of the Milky Way with an assumed distance to the galactic center of 8 kpc (Honma, Sofue 1997). Assuming the same distance, the jet's top (G50−26) is as high as $z = -3.4$ kpc from the galactic plane, and its projected length is about 4.5 kpc and width 300 pc. Wakker and van Woerden (1991) estimate the total H I mass to be $\sim 2.4 \times 10^5\,M_\odot$ for a distance of 6.5 kpc; we, therefore, adopted a mass of $\sim 2.7 \times 10^5\,M_\odot$ for 6.9 kpc. The gravitational energy required to lift the mass to the height is a few times 10^{52} erg. The averaged gas density in the whole jet of 4 kpc × 300 pc in length and width, respectively, is of the order of $n_{\rm H} \sim 0.08\,\mathrm{H\,cm^{-3}}$. The peak-intensity position is at G39−13.5, where the integrated H I intensity is measured to be $I_{\rm HI} = 177\,\mathrm{K\,km\,s^{-1}}$, corresponding to a column density of H I atoms of $N_{\rm H} = 3.2 \times 10^{20}\,\mathrm{H\,cm^{-2}}$. If we assume a line-of-sight depth of ~ 300 pc, the H I density at this peak position is on the order of $n_{\rm H} \sim 0.3\,\mathrm{H\,cm^{-3}}$.

In order to see the kinematics of the H I jet, we show position–velocity diagrams along and across the H I jet G40−15 in figure 4a and b, respectively. Figure 4a shows a wavy variation of the center velocity with an amplitude of a few $\mathrm{km\,s^{-1}}$. Figure 4b shows that the H I jet is rotating in the same sense as the galactic rotation, as indicated by the thick line. The rotation is expected from a magnetic twisting jet model, as proposed in section 3.

We further examined local variations of the velocity due to the internal motion and rotation by making a velocity-field map, as shown in figure 5. Thereby, we first made three gray-scale maps of the H I intensity at $V_{\rm LSR} = 100$, 90, and $80\,\mathrm{km\,s^{-1}}$, and then colored them by *R* (red), *G* (green), and *B* (blue) colors, respectively. We added the three maps to obtain a color-coded intensity map, where the brightness indicates the intensity and the *RGB* colors represent velocity shifts from $90\,\mathrm{km\,s^{-1}}$ with *R* being redshifted by $+10\,\mathrm{km\,s^{-1}}$, *G* at center, and *B* blueshifted by $-10\,\mathrm{km\,s^{-1}}$. In addition to the major G40−15 structure with the velocity features shown in the P–V diagrams, there appear numerous spurs and strings emanating from the galactic plane toward high latitudes. Most prominent is a very narrow and long string that twines around the jet of G40−15, and the radial velocity changes semi-periodically along the string. The string appears to be tangled at G38−18 to form a helical feature. These properties suggest that the string is a magnetic helical tube extending from the galactic plane associated with some twisting motions.

We have searched for associated emissions in other wavebands with the G40−15 H I jet in order to estimate the magnetic strength and molecular gas mass. First of all, we tried to estimate the magnetic field strength from radio continuum emission. However, a background-filtered radio continuum map at 408 MHz, as processed from the Bonn–Parkes survey (Haslam et al. 1982), showed no significant continuum emission associated with the H I jet due to the bright and noisy galactic disk emission. We could only give an upper limit to the brightness temperature of $\Delta T_B \sim 6$ K, or $\Sigma \sim 3 \times 10^{-22}\,\mathrm{W\,m^{-2}\,str^{-1}\,Hz^{-1}}$ at 408 MHz toward G40−15. This yields a volume emissivity of $\epsilon \sim 10^{-25}\,\mathrm{erg\,cm^{-3}\,s^{-1}}$ for a line-of-sight length of ~ 300 pc. If we assume an equipartition of the energy densities of the magnetic fields and comic-ray electrons, we could thus estimate a rough upper limit to the magnetic field strength of $B \lesssim 20\,\mu$G. We then tried to measure the dust content by examining the IRAS 60 μm data, but could not find any particular dust feature, mainly because of the too noisy background in the data.

Finally, in order to estimated associated molecular gas mass, we performed CO (J = 1–0) line observations toward several points in the H I-densest part at G39−14 in 1999 August, using a 4-m mm-wave telescope, NANTEN, at Las Campanas Observatory, Chile operated by Nagoya University (Fukui et al. 1999). An upper limit to the column density of molecular hydrogen of a few-times 10^{19} $\mathrm{H_2\ cm^{-2}}$ was obtained for a CO intensity-to-$\mathrm{H_2}$ conversion factor of 2×10^{20} $\mathrm{H_2\ cm^{-2}\ [K\,km\,s^{-1}]^{-1}}$. This yields an upper limit to a molecular

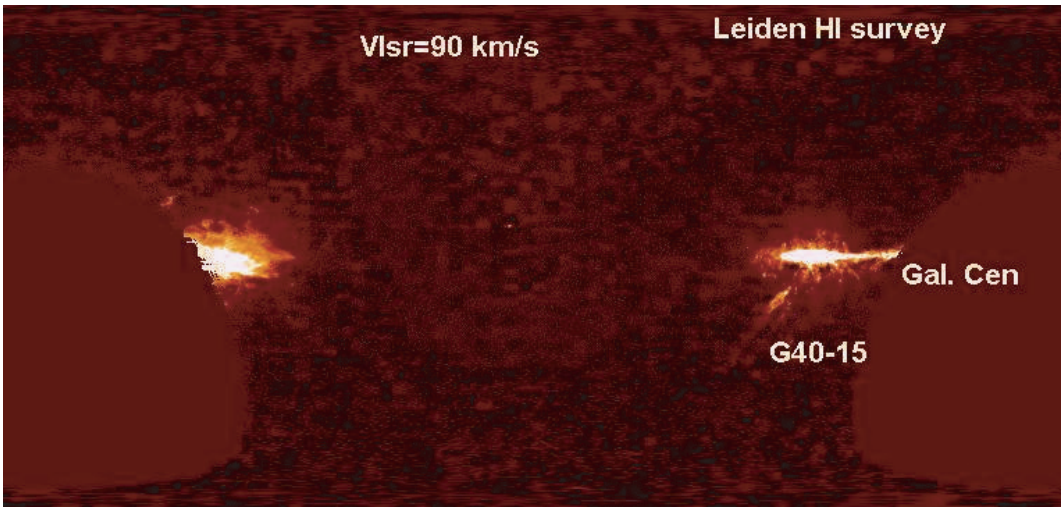

Fig. 1. H I map of the whole sky at $V_{LSR} = 90\,km\,s^{-1}$ (Hartman, Burton 1997).

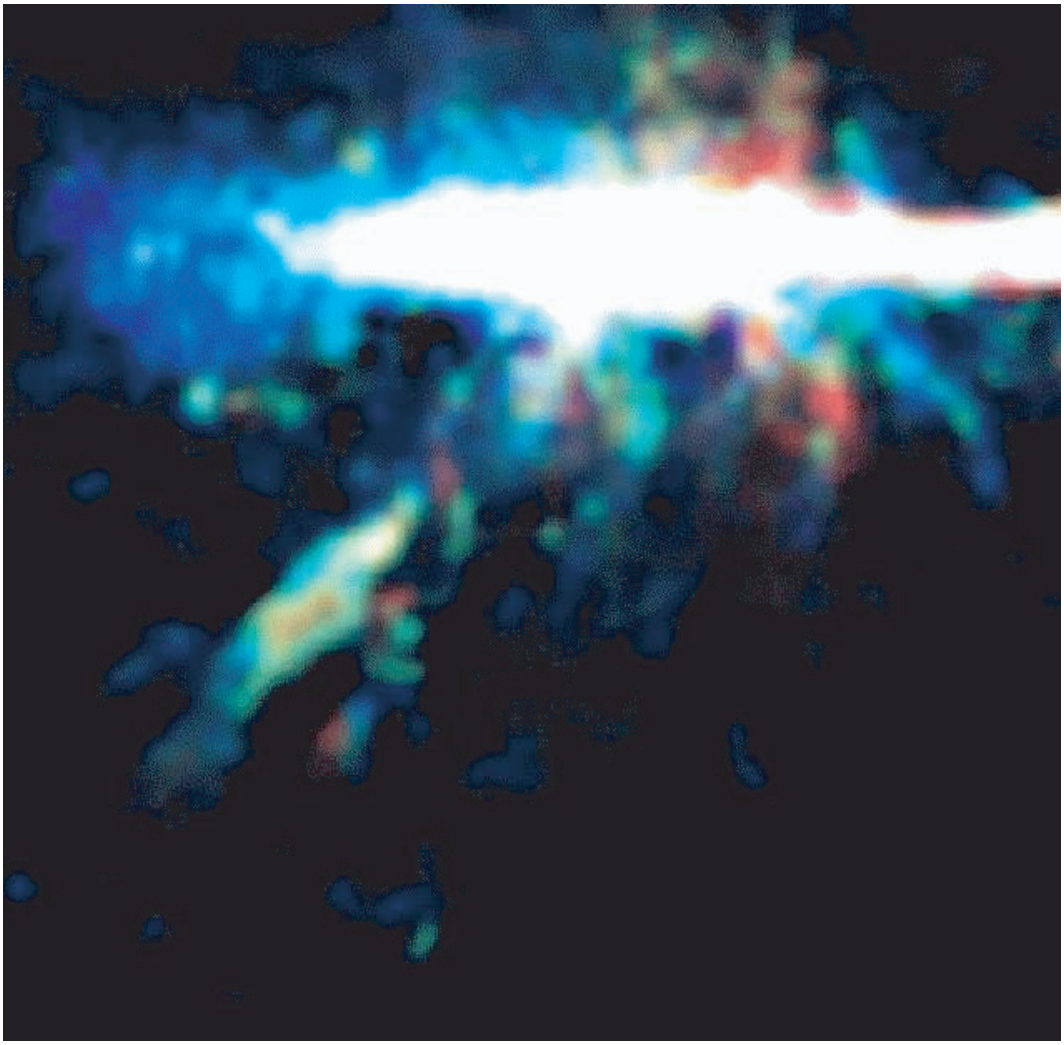

Fig. 5. Color-coded H I map of G40−15 and its surroundings. The *R*, *G*, and *B* colors correspond to red- ($+10\,km\,s^{-1}$), green- ($0\,km\,s^{-1}$), and blue-shifts ($-10\,km\,s^{-1}$) from the center velocity of G40−15 ($V_{LSR} = 90\,km\,s^{-1}$).

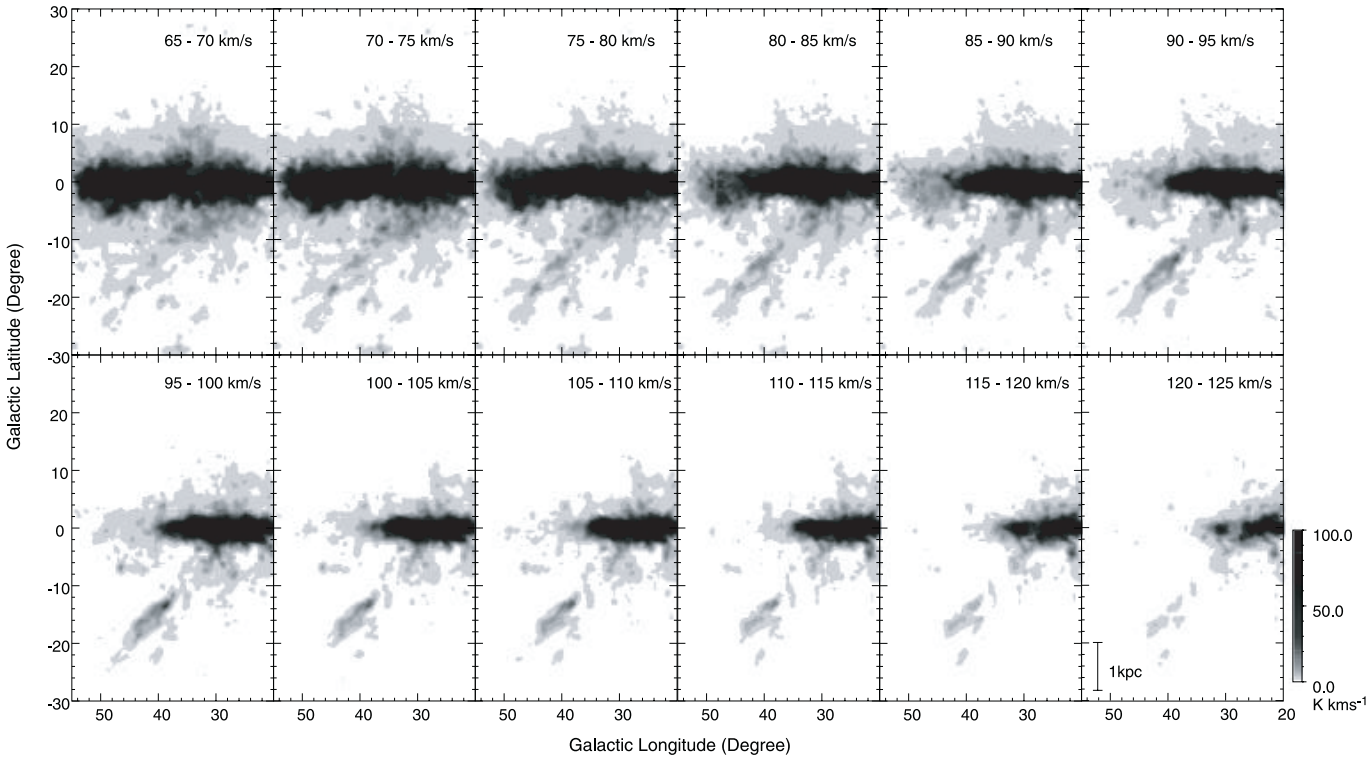

Fig. 2. H I channel maps integrated every 5 km s^{-1} interval. The H I jet G40−15 is seen most clearly at $V_{\rm LSR}$ = 90 to 100 km s^{-1}.

mass of several-times $10^4\,M_\odot$ for the 2 kpc × 0.2 kpc region around G40−15. The molecular fraction is, therefore, less than 0.1, which is normal for a high-altitude and low-density region out of the galactic disk (Imamura, Sofue 1997).

3. Magnetic Jet Model of the H I Spur G40−15

The coherent and straight nature of G40−15 suggests that the jet is a magnetic structure. We tried to interpret the G40−15 H I jet as a twisting magnetic jet, and performed an MHD simulation of a jet from a magnetized collapsing cloud.

3.1. Straight Jet Structure Indicating a Magnetic Tube

The H I jet G40−15 is unique for its radial velocity being close to the terminal velocity of the 4-kpc molecular ring. The error in the kinematical distance can be minimized, and the distance has been determined to be 6.9 kpc. Consequently, the spur is the most extended coherent vertical structure of neutral hydrogen in the Galaxy so far found. The spur's top is 3.4 kpc high from the galactic plane, and the whole structure is 4.4 kpc long. Hence, H I jet G40−15 is an ISM structure penetrating deeply into the galactic halo, linking the disk and halo. In the following, we discuss possible origins of this prominent H I spur.

The narrow and straight morphology with a length of several kpc suggests that the structure is controlled by magnetic fields. A twisted magnetic jet mechanism (Shibata, Uchida 1987) due to strong shear motion in the galactic shock wave could accelerate such a straight streaming. The upward acceleration of gas occurs when the vertical Alfvén velocity exceeds the local gravitational velocity. The vertical Alfvén velocity is given by

$$V_{\rm A} = B_\phi/\sqrt{4\pi\rho} \sim 10^2 \left(\frac{\rho}{0.01 m_{\rm H}\,{\rm cm}^{-3}}\right)^{-1/2} \left(\frac{B_\phi}{5\mu{\rm G}}\right)\ {\rm km\,s^{-1}}, \qquad (1)$$

where ρ is the density of gas in the magnetic tube, and B_ϕ is the azimuthal strength of the magnetic field. If we take $\rho \sim 10^{-2} m_{\rm H}$ cm^{-3} and $B_\phi \sim 10\,\mu$G, which is consistent with the estimated upper limit from the radio continuum as above, the Alfvén velocity is $\sim$200 km s^{-1}. The gravitational infalling velocity from 3 kpc height is of the same order of magnitude or less. Hence, if the azimuthal strength of the twisted magnetic field is greater than 10 μG and/or the gas density within the magnetic tubes is less than $\sim 0.01 m_{\rm H}$ cm^{-3}, an upward acceleration of the H I gas to the observed height is possible. Such an enhanced magnetic flux will be produced by shock compression of interstellar gas along dense spiral arms, such as the 4-kpc molecular ring.

Strong shock compression of a spinning molecular cloud penetrated by a magnetic field will cause a twisted magnetic jet by a mechanism presented by Shibata and Uchida (1987). In fact, an integrated H I intensity map between 80 and 120 km s^{-1} shows another twisted H I ridge, spiraling around the lower latitude part of G40−15, as shown in figures 3 and 5. Such a twisting interaction of two gaseous spurs may be understood, if they are magnetic-tubes interacting with each other in shearing motion due to the differential rotation of their roots

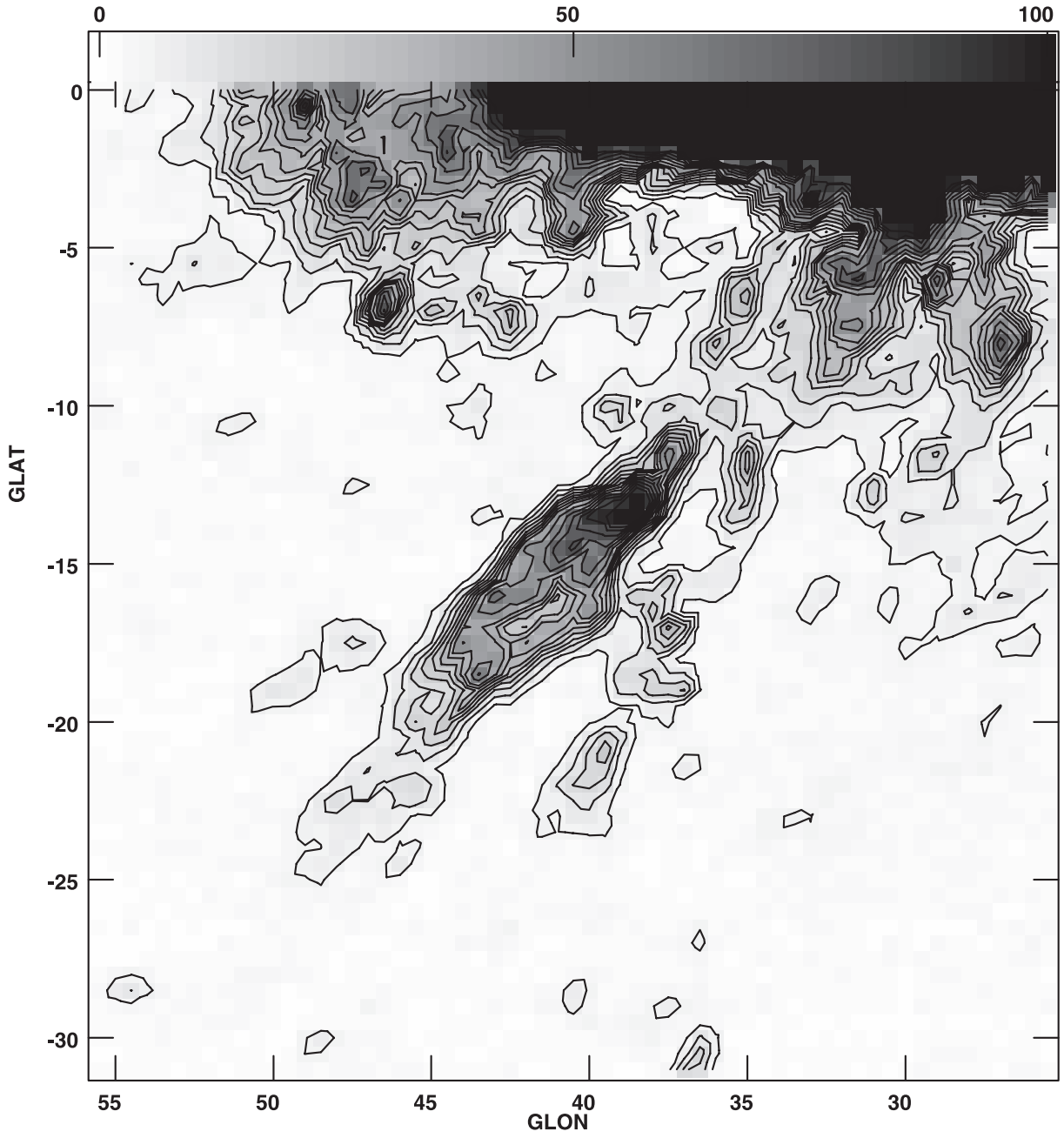

Fig. 3. Integrated H I map between 80 and 120 km s^{-1} with contours drawn at 5, 10, 20, 40, 80, and 160 K km s^{-1}.

anchored to a massive interstellar cloud. If the cloud is rotating and penetrated by a magnetic field, a twisting magnetic jet may be produced, which accelerates the H I jet.

3.2. Spinning Cloud in the G30−00 Complex

We examined the gas distribution and kinematics of the root of the H I jet at G30−00, which positionally coincides with the tangential point of the 4-kpc molecular ring. Figure 6 (top) shows a longitude–velocity (L–V) diagram in H I along the galactic plane around G30, reproduced from the H I data by Hartmann and Burton (1997), and figure 6 (bottom) the same, but for CO line emission taken from Dame et al. (2001). There is a massive cloud found both in H I and CO at G30 and $V_{\rm LSR} = 90$ km s^{-1}, coinciding with the tangential point of the 4-kpc ring. The complex is associated with a massive molecular cloud at the same place and velocity (Dame et al. 2001). As shown by the thick lines, the H I cloud is spinning at a rate of 20 km s^{-1}/150 pc, and the CO cloud at 20 km s^{-1}/60 pc. The spin directions are the same as the galactic shear motion (anticlockwise, as seen from the northern galactic pole). The molecular cloud has a smaller extent and is rotating faster than the H I cloud.

The rotation energy of the cloud, which is rotating at ~ 10 km s^{-1} and has a mass of $\sim 1.5 \times 10^6\, M_\odot$ as inferred from the H I and CO luminosities, is estimated to be $\sim 2 \times 10^{51}$ erg. Therefore, rotation energy of the G30−00 cloud is

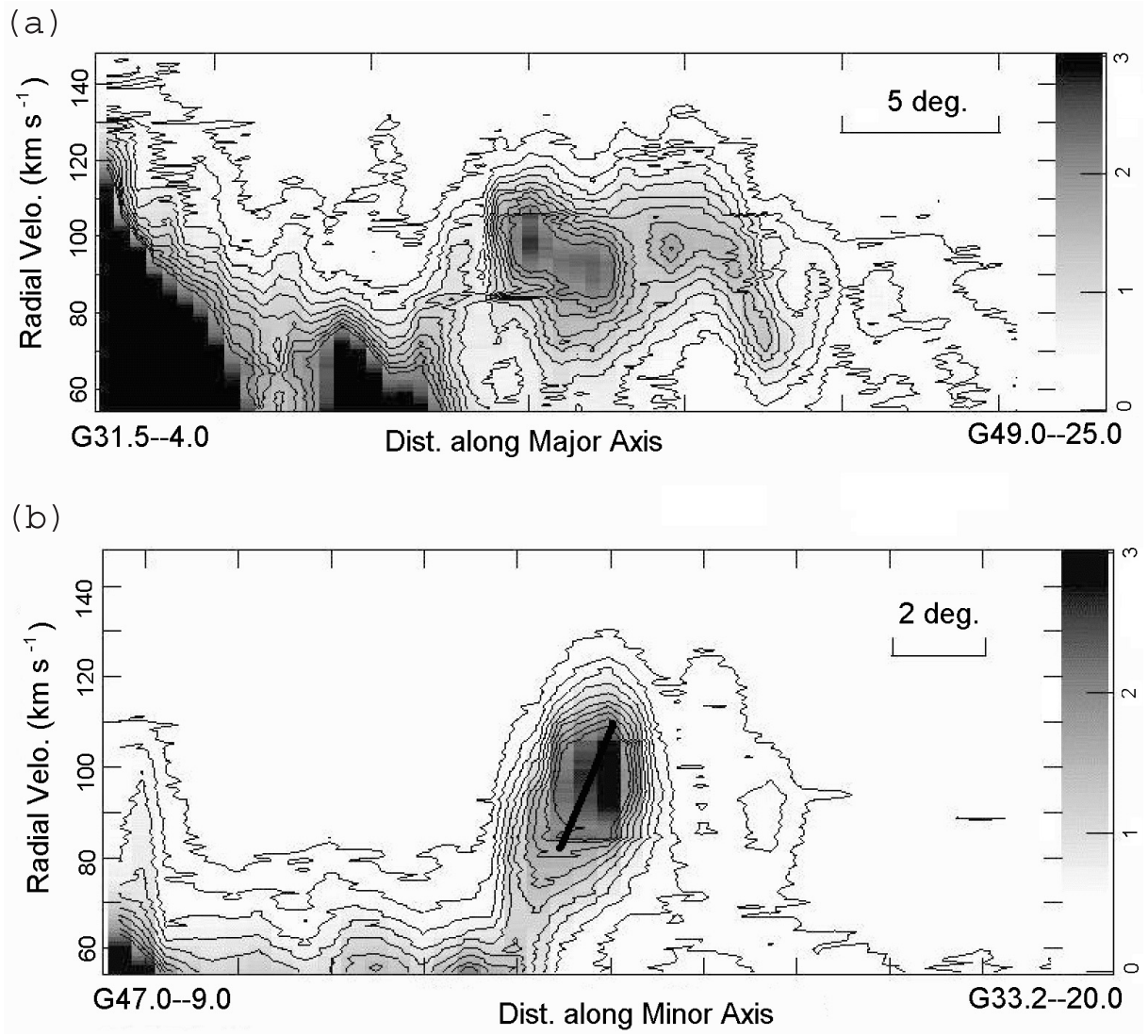

Fig. 4. (a) (top) Position–velocity diagram along the major axis of H I jet G40−15 from G31.5−4.0 (left) to G49.0−25.0 (right) across G40−15. The tick interval is 5°. The galactic plane is to the left. Contours are drawn at 0.25 K interval. (b) (bottom) Position–velocity diagram perpendicular to H I jet G40−15 across G40−15 from G47.0−9.2 (left) to G33.2−20.0 (right), showing rotation, as indicated by the thick line. The ordinate tick interval is 2°. Contours are drawn at 0.25 K intervals.

comparable to the gravitational energy of the H I jet G40−15. The high-velocity rotation can be accelerated by a galactic shock compression of a spinning cloud, when it encounters the 4-kpc arm. In fact, Fujimoto and Tanahashi (1971a,b) showed that galactic H I clouds are rotating around their arbitrary spin axes. In the present case for G30−00, the spin direction is in the same direction as the shear motion due to galactic rotation, but the spin rate is much faster than the usual shear motion. This can be understood as being due to an acceleration of rotation by the shock compression and angular-momentum conservation of the cloud.

3.3. MHD Simulation of a Magnetic H I Jet

If a spinning interstellar cloud is penetrated by a magnetic field, the cloud will twist the field lines and accelerate a twisting magnetic jet (Shibata, Uchida 1986, 1987; Kudoh et al. 1998, 1999). The acceleration of the jet results in a loss of angular momentum of the cloud, which accelerates the collapse of the cloud, while further accelerating the jet. We thus made an MHD simulation of this accelerating mechanism. We assumed ideal MHD in axial symmetry, and modeled a local region of the Galaxy. We used axially symmetric cylindrical coordinates (R, z), where R represents the distance from the axis and z the vertical distance from the equator of the cloud. The specific heat ratio, γ, is assumed to be $\gamma = 5/3$.

The cloud's gravity is approximated by a Plummer's potential with a softening radius representing the cloud's size,

$$\Psi_{\rm P} = -\frac{GM}{\sqrt{R^2 + z^2 + b^2}}, \tag{2}$$

where G is the gravitational constant, M the mass of the gravitational source, and b the softening radius. Here, we took $M \simeq 10^6\, M_\odot$ and $b \simeq 10\,$pc.

As the initial condition, we assumed a disk-shaped cloud.

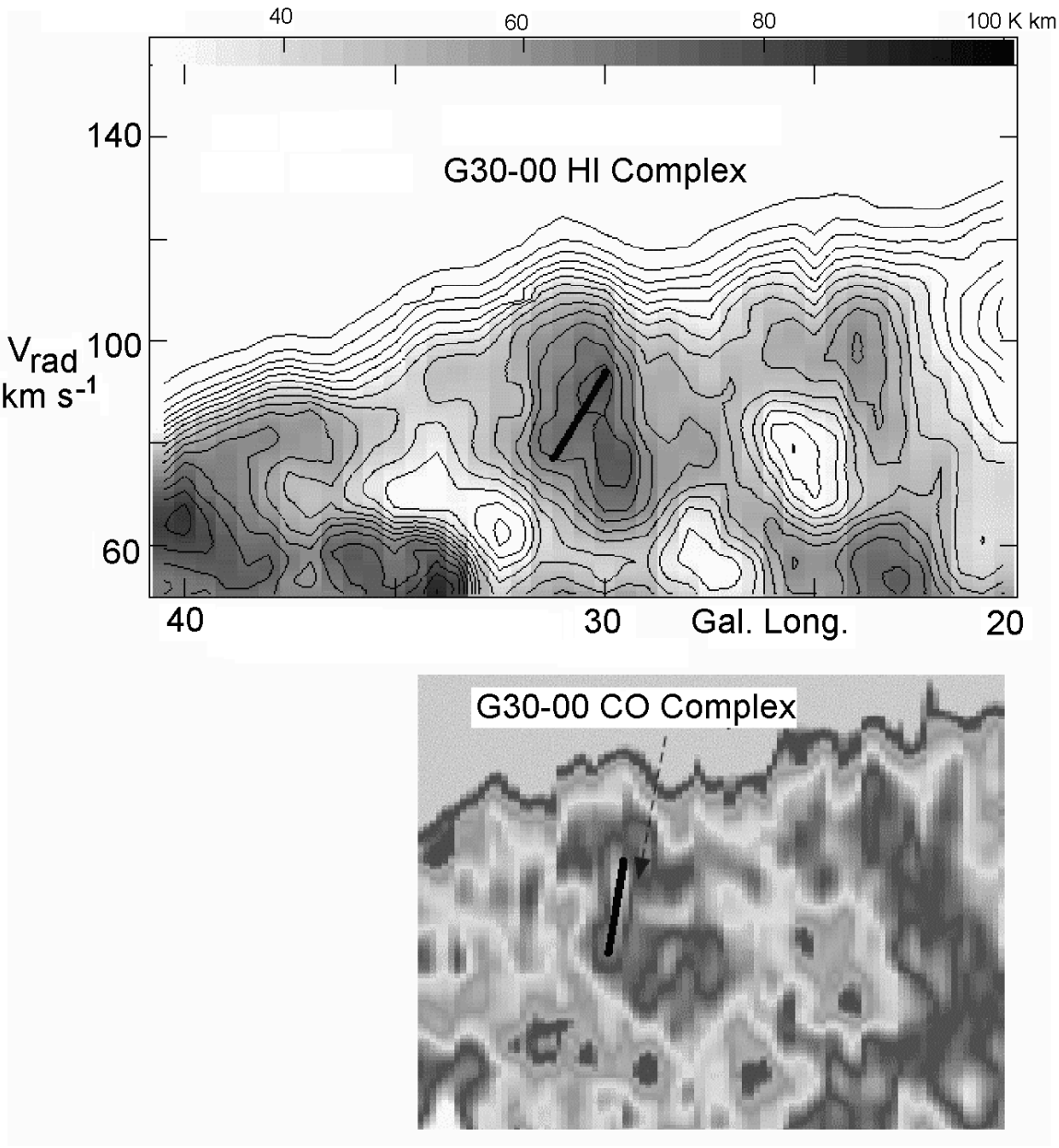

Fig. 6. (Top) Longitude–velocity diagram for H I line emission (Hartman, Burton 1997) along the galactic plane across the Scutum tangent of the 4-kpc molecular ring around G30−00. Note the giant H I cloud, indicated by the thick line, showing a rapid spin motion in the same sense as the galactic rotation, is probably due to acceleration by shock compression under angular-momentum conservation. (Bottom) The same for CO line emission.

The density and pressure distributions were determined by the equilibrium state of rotating gas in the Plummer's potential,

$$\Psi_{\rm P} + \Psi_{\rm c} + (n+1)\frac{P}{\rho} = \text{constant}, \tag{3}$$

where we assumed polytropic relation, $P = K\rho^{1+1/n}$, with $n = 3$ for the initial condition (e.g., Matsumoto et al. 1996). In equation (3), $\Psi_{\rm c}$ is a centrifugal potential. We assumed that $\Psi_{\rm c}$ (and rotation speed v_ϕ) is a function of R only:

$$\Psi_{\rm c} \equiv -\int \frac{v_\phi^2}{R} dR = \begin{cases} \dfrac{GM}{\sqrt{R^2+b^2}} & (R \le R_0). \\ L_0 R^{-2(1-a)} + K_0 & (R > R_0). \end{cases} \tag{4}$$

In equation (4), L_0 and K_0 were determined that $\Psi_{\rm c}$ and $d\Psi_{\rm c}/dR$ were continuous at $R = R_0$. We choose $R_0 = 4b$ and $a = 0$ in this paper. The cloud density and pressure are determined by solving equation (3) with Plummer's gravitational potential of equation (2) and the centrifugal potential of equation (4). The rotation speed of the cloud comes from equation (4). In the cloud, we assumed $C_{\rm sc}^2/(\gamma V_{K0}^2) = 0.002$,

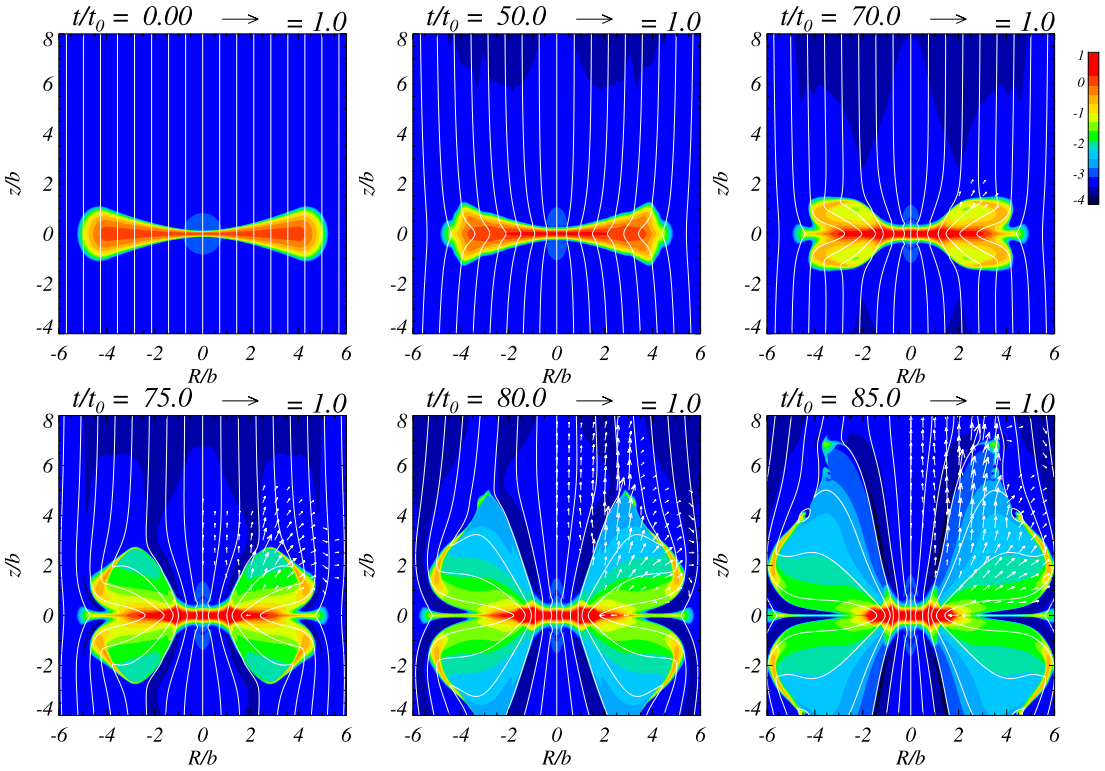

Fig. 7. Time evolution of the gas density in a magnetized twisting jet from a collapsing cloud. The density is normalized by $\rho_0 \simeq 10^3\,\mathrm{H\,cm^{-3}}$. The white lines show the poloidal magnetic field lines. The arrows show poloidal velocity vectors, which are normalized by $V_{K0} = (GM/b)^{1/2} \simeq 21\,\mathrm{km\,s^{-1}}$. The arrows are shown only for the region of $R > 0$ and $z > 0$. The unit of length is $b \simeq 10\,\mathrm{pc}$ and the unit of time is $t_0 = b/V_{K0} \simeq 4.7 \times 10^5\,\mathrm{yr}$. Note that the time interval is not uniform.

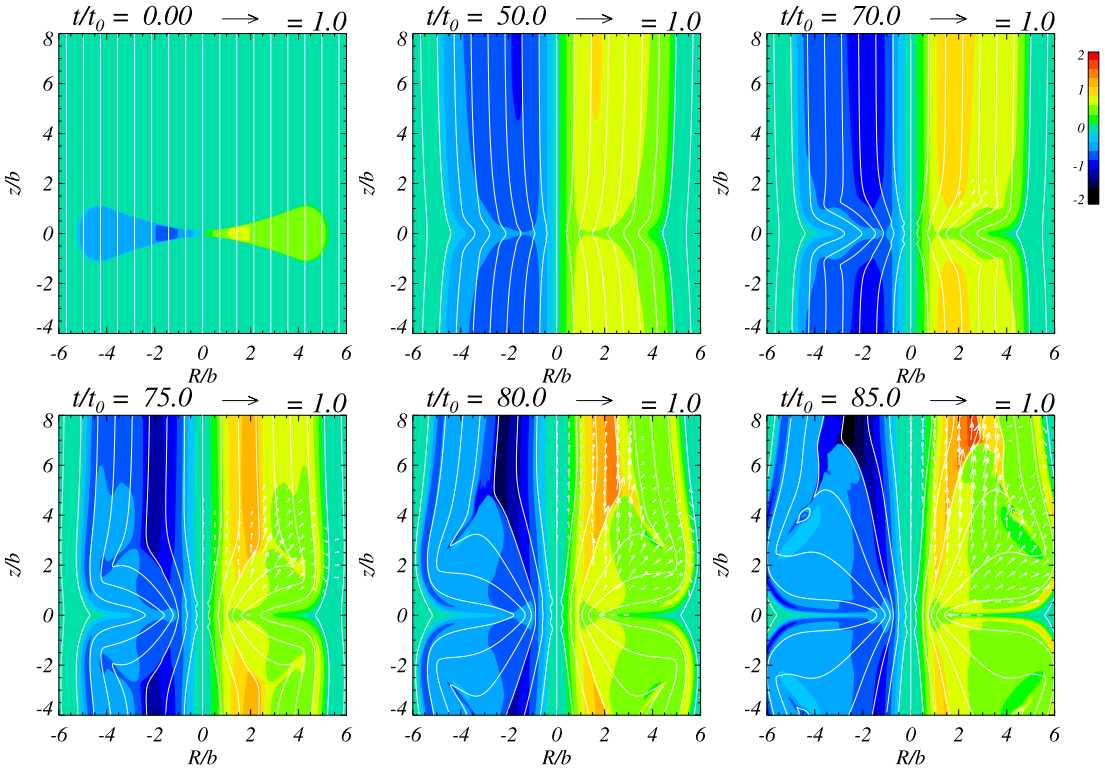

Fig. 8. Time evolution of the rotation speed of gas in a magnetized twisting jet. The rotation speed is normalized by $V_{K0} = (GM/b)^{1/2} \simeq 21\,\mathrm{km\,s^{-1}}$. The white lines show the poloidal magnetic field lines. The arrows show the poloidal velocity vectors, which are normalized by V_{K0}. The arrows are shown only for the region of $R > 0$ and $z > 0$. The unit of length is $b \simeq 10\,\mathrm{pc}$ and the unit of time is $t_0 = b/V_{K0} \simeq 4.7 \times 10^5\,\mathrm{yr}$. Note that the time interval is not uniform.

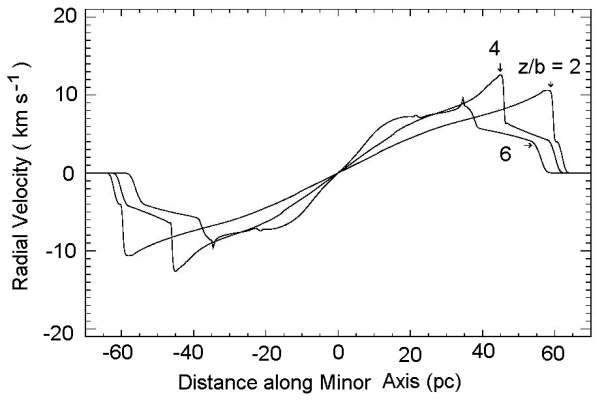

Fig. 9. Density-weighted position–velocity diagram across the simulated MHD jet at three heights, as indicated by the distances z from the cloud rotation plane.

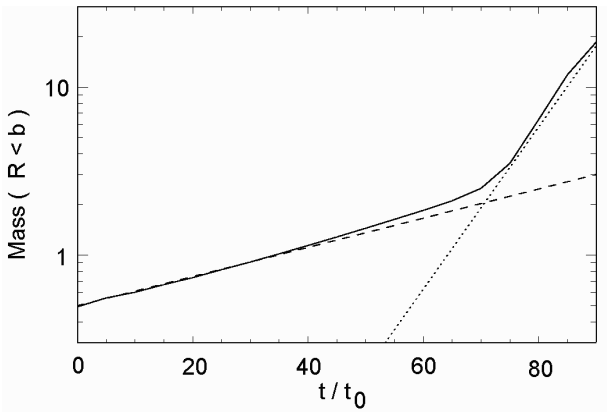

Fig. 10. Time evolution of the mass within $R < b$. The mass is normalized by $\rho_0 b^3$. The solid line shows the simulation result. The dashed line is proportional to $\exp(t/50t_0)$, and the dotted line to $\exp(t/9t_0)$. Note the acceleration of cloud collapse after $t/t_0 \sim 70$.

where $C_{\rm sc}$ is the initial sound speed in the cloud at $(R, z) = (b, 0)$ and $V_{K0} = (GM/b)^{1/2}$, respectively. The size of the cloud was determined where the solution of the density becomes positive.

Outside of the cloud, we initially assumed gravitationally equilibrium isothermal gas without rotation. In the ambient gas, we assumed $C_{\rm sa}^2/(\gamma V_{K0}^2) = 1.0$, where $C_{\rm sa}$ is the initial sound speed in the ambient gas. The gas density of the cloud was taken to be $\rho_0 \simeq 10^3 m_{\rm H}\,{\rm cm}^{-3}$ at $(R, z) = (b, 0)$ and the ambient gas density $\simeq 1 m_{\rm H}\,{\rm cm}^{-3}$ at $(R, z) = (0, 0)$. The cloud and ambient gases were initially embedded in a uniform vertical magnetic field of $B_0 \simeq 1.3 \times 10^{-5}$ G, running parallel to the spin axis of the cloud. The magnetic pressure was of the same order as the gas pressure in the cloud.

We used an MHD code developed for the formation of astrophysical magnetic jets (Kudoh et al. 1998, 1999). The minimum grid size was $0.02\,b$ in both the R and z directions. We gradually increased the grid size where $R > 6b$ and $z > 7b$. The computational region is about $0 \le R \le 9.8b$ and $0 \le z \le 254b$. The mirror symmetrical boundary condition was assumed about the equatorial plane. The outer boundary conditions were free boundaries for both the R and z directions.

Figure 7 shows the time evolution of the gas density. The density was normalized by ρ_0. Figure 8 shows the time evolution of the rotation speed. The rotation speed is normalized by $V_{K0} = (GM/b)^{1/2} \simeq 21\,{\rm km\,s}^{-1}$. The white lines show poloidal magnetic field lines. The arrows show poloidal velocity vectors, which are normalized by V_{K0}. The unit of length is b and the unit of time is $t_0 = b/V_{K0} \simeq 4.7 \times 10^5$ yr. One rotation time of the cloud at $R = b$ is $\simeq 10.6 t_0$. The cloud loses its angular momentum through the magnetic field, and gradually contracts in $t/t_0 = 0$–70. After several rotations of the cloud ($t/t_0 \simeq 70$), a part of the cloud is ejected by magnetic force. It forms a collimated flow of gas along the poloidal magnetic filed lines ($t/t_0 = 75$–85), which we may call a magnetic jet. The rotation speed of the ejected mass is on the order of $10\,{\rm km\,s}^{-1}$.

Figure 9 shows a position–velocity diagram across the simulated magnetic jet at $z = 2b$, $4b$, and $6b$, where the radial velocity has been calculated using $v_r = \int \rho v_y dy / \int \rho dy$, where y is the distance along the line of sight. The rotation is nearly rigid, and the simulated P–V diagram mimics the observed one, as shown in figure 6.

According to the loss of angular momentum due to the magnetic jet, the cloud contraction develops gradually in the first several rotations at $t/t_0 = 0$–70. In this stage, the loss of angular momentum of the cloud is caused only by magnetic braking of non-linear torsional Alfvén waves produced by the rotation of the cloud. The magnetic braking time of the initial condition is roughly estimated to be $(Z/V_{\rm A,a})(\rho_{\rm c}/\rho_{\rm a}) \sim 100 t_0$, where Z is a half thickness of the cloud, $V_{\rm A,a}$ is the Alfvén velocity of ambient gas, $\rho_{\rm c}$ is the cloud density and $\rho_{\rm a}$ is the density of ambient gas (Mouschovias, Paleologou 1980). Once a part of the cloud is ejected, however, the cloud contracts more rapidly ($t/t_0 \ge 70$). The angular-momentum transfer becomes more efficient as the jet evolves because of the increase of mass ejected into the ambient gas. This is evidently shown in the P–V diagrams in figure 9 for the ejected gas.

Figure 10 shows the variation of the cloud mass within $R < b$ as a function of time. This diagram shows a rapid increase of mass after the mass ejection ($t/t_0 \ge 70$). The dashed line is proportional to $\exp(t/50t_0)$ and the dotted line proportional to $\exp(t/9t_0)$, which are shown for a comparison with the simulation. The growth time of the central mass is approximately equal to the braking time on the first stage. As the mass ejection proceeds, the growth time becomes about the same as the rotation time of the cloud. This implies that the collapse of the cloud core is drastically accelerated after growth of the magnetic twisting jet.

The simulation thus proved that the twisting-magnetic jet mechanism and the associated collapse work in the present condition of the interstellar cloud. However, since the calculation was limited to the initial ~ 10 rotation periods, the jet grew to a height of the cloud size. Moreover, the gravitational potential was fixed, and no self-gravity was taken into account, which resulted in a softer collapse. If the self-gravity is taken into account, the loss of angular momentum of the cloud will result in a further acceleration of the gravitational collapse, and will lead to the acceleration of a stronger and longer jet.

3.4. *Collapse of a Cloud by a Magnetic Jet and Star-Cluster Formation*

Our MHD simulation showed that a magnetized spinning interstellar cloud collapses by the loss of angular momentum through the acceleration of a twisting magnetic jet. As the jet grows, the loss of angular momentum leads to further acceleration of the collapse. This process acts as a mechanism not only to eject a magnetic jet, but also to accelerate the gravitational collapse of a cloud to form a dense core by the self gravity. If a cloud of $M = 10^6\,M_\odot$ collapses to a very dense cloud of radius $r = 1$ pc, the released gravitational energy is on the order of $E \sim GM^2/r \sim 10^{53}$ erg. This is significantly greater than the energy required to lift the G40−15 H I jet to its present height. Energetically, it is possible to accelerate the H I jet G40−00 by the collapse of a massive magnetized cloud. In fact, our MHD simulation showed that the mechanism works well in its initial phase. This collapsing mechanism of a molecular cloud will be effective in such a strongly shocked and turbulent region as the 4-kpc molecular ring.

The formed dense molecular core will be gravitationally unstable against fragmentation into denser protostellar clouds, and may result in a bursting formation of stars. A cluster of stars of some $10^5\,M_\odot$ will be formed in a compact few pc region, even if the star-formation efficiency is about on the order of $\sim 10\%$ and the initial cloud mass is $\sim 10^6\,M_\odot$. We, thus, propose a formation mechanism of a globular cluster due to the magnetic-jet collapse of a magnetized molecular cloud. This mechanism mimics the molecular bipolar flow phenomenon associated with star-formation regions (Bally, Lada 1983), where the angular momentum of a collapsing proto-stellar disk is extracted through acceleration of a twisting magnetic jet (Uchida, Shibata 1985).

Our new view concerning the formation of a dense star cluster, possibly a globular cluster, is consistent with the observational facts known in the vicinity of G30−00: A giant molecular cloud, as massive as $1.4 \times 10^6\,M_\odot$, is present at G30.8−0.05 with $V_{\rm lsr} = 92\,{\rm km\,s^{-1}}$, coinciding positionally and kinematically with the tangent point of the 4-kpc ring (Dame et al. 2001). An H I complex having a mass of $\sim 10^5\,M_\odot$ is associated with the molecular cloud (Hartman, Burton 1997). An intense H II region with the thermal radio source W 43, having a peak emission measure as high as $7.2 \times 10^5 {\rm cm^{-6}\,pc}$ and a recombination-line radial velocity of $90\,{\rm km\,s^{-1}}$ (Downes et al. 1980), is tightly associated with this molecular cloud, indicating intense star formation in the cloud (Ikuta, Sofue 1997). A bow-shock feature is observed in the radio continuum and CO-line emission extending from this H II region, indicating a strong galactic-shock compression of the 4-kpc arm (Sofue 1985), and therefore, compression of molecular clouds, leading to a spinning-up of their rotation.

4. Discussion

We have noticed a giant H I jet G40−15, and interpreted it as one of numerous H I spurs emanating from the galactic plane. Our view is quite different from those proposed for this "Smith cloud" by assuming that the feature is one of high-velocity clouds out of the galactic plane (e.g., Bland-Hawthorn et al. 1998). In our view, G40−15 is a coherent H I structure at high altitude, 4.5 kpc in length and 300 pc in width. Its root at the galactic plane positionally as well as kinematically coincides with the Scutum tangent of the 4-kpc molecular ring at G30−00 (Dame et al. 1987, 2001). For its coherent, long structure, we immediately supposed that the structure may be due to some magnetic-jet mechanism. We thus proposed a twisting magnetic jet model for the formation, and performed an MHD simulation of a twisting magnetic jet from a collapsing rotating gas cloud. We indeed found a massive rotating molecular cloud at G30−00. By a simulation, we showed that the collapse of a cloud is accelerated by the ejection of a magnetic jet. We also showed that a dense gas core grows in the central part of a giant molecular cloud by effective extraction of angular momentum through a twisting magnetic jet. We further proposed a new formation scenario of a compact stellar cluster, or a globular cluster, from such a massive dense core of a few pc radius.

If we assume that the H I spur G40−15 is a galactic object, some alternative interpretation could be possible. We comment on such possibilities.

3D Galactic Shock Wave: High-Altitude Bow Shock: The root of G40−15 jet in the galactic plane at G30−00 positionally coincides with the tangential direction of the 4-kpc molecular ring. In this direction, there exists an active star-forming region associated with the H II region W 43, whose galactic coordinates are G30.8−00.0. A prominent bow-shock feature in 10 GHz radio continuum has been reported to be associated with W 43 at G30.5−00 (Sofue 1985), which draws a bow-shaped radio ridge concave to the H II region, extending toward G40−15 and is interpreted as being due to a bow shock produced by a galactic shock wave in the 4 kpc ring (arm). This coincidence suggests that H I jet G40−15 could be a high-altitude extension of the galactic bow shock. In fact, a hydrodynamical simulation predicts a bow shock at high altitudes in the galactic halo (Martos et al. 1999). The high velocity dispersion can be understood as due to its large line-of-sight depth, because it is a tangential view of a leaned H I wall curving along the 4-kpc arm. If we assume a line-of-sight depth of ~ 1 kpc at G40−15, the mean gas density in the spur is only $\sim 0.1\,{\rm H\,cm^{-3}}$. Also, galactic shock wave theory predicts that the radial velocity in the lower-longitude (pre-shock stream) side is higher, jumping into lower velocities at the higher longitude (post-shock, down stream) side (Fujimoto 1966; Roberts 1969). This is consistent with the apparent rotation of the H I spur in the same sense as the galactic rotation. In this theory, the observed H I gas is not necessarily supplied from the galactic disk, and hence, no extra energy to lift the mass is required. However, this theory predicts a positive-latitude counter spur, while we find no clear evidence of this positive-latitude counterpart. We find only a very weak H I jet G38+10 seen in the H I map around $V_{\rm LSR} = 100\,{\rm km\,s^{-1}}$.

Shock Wave from the Galactic Center: A bipolar hyper-shell (BHS) model has been proposed for the North Polar Spur (NPS), in which a dumbbell-shaped shock front is formed by a starburst at the galactic center (Sofue 1994, 2000; Sofue, Vogler 2001). Galactic-center starbursts would have occurred intermittently, and a BHS shock from a former starburst may still be propagating in the outer halo and disk, and will be

observed as leaned radio spurs. Moreover, such a long-lived shock front would focus on the disk, compressing the interstellar gas, and form a ring-like density enhancement in the disk. A compressed gaseous ring will be associated with a BHS in the halo, which would mimic the 4-kpc molecular ring associated with H I jet G40−15 and its positive-latitude weak counter spur, G38+10. Since the shock wave may already be decelerated to low velocities to keep the gas neutral, no X-ray emission is expected. However, the shock could enhance radio continuum emission in the halo, but no radio spurs are found in coincidence with H I jet G40−15 in the 408 MHz survey (Haslam et al. 1982). Also, another question remains why G40−15 is exceptionally strong compared to the other root positions of the BHS, such as the North Polar Spur, whose root is at around G20 where no prominent H I feature has been reported.

Among these possibilities, we, thus, prefer the magnetic-jet model for G40−15, because of its unique features: an extremely straight and narrow structure, and apparent and kinematical coincidence of the root with the 4-kpc ring associated with a rotating massive cloud at G30−00.

We have assumed that G40−15 is a galactic object because of the apparent and kinematical connection to the 4-kpc ring at G30−00, which allowed us to estimate an accurate distance. However, as discussed in section 1, we cannot reject the possibility that G40−15 is a high-velocity cloud at extragalactic location or beyond the galactic disk. In this case, the coincidence of the recession velocity with that of the galactic rotation is only by chance, and the distance should be determined by another means in order to discuss the physical nature.

Numerical computations were carried out on the VPP5000 at the Astronomical Data Analysis Center in the National Astronomical Observatory of Japan. We are grateful to Dr. K. Ohnishi of Nagoya University for his help in CO observations using the 4-m mm-wave telescope at Las Campanas Observatory, Chile operated by Nagoya University.

References

Bally, J., & Lada, C. J. 1983, ApJ, 265, 824
Bland-Hawthorn, J., Veilleux, S., Cecil, G. N., Putman, M. E., Gibson, B. K., & Maloney, P. R. 1998, MNRAS, 299, 611
Dame, T. M., et al. 1987, ApJ, 322, 706
Dame, T. M., Hartmann, D., & Thaddeus, P. 2001, ApJ, 547, 792
Downes, D., Wilson, T. L., Bieging, J., & Wink, J. 1980, A&AS, 40, 379
Fujimoto, M. 1966, in IAU Symp. 29, Non-Stable Phenomena in Galaxies, ed. M. Arakeljan (Yerevan: Nauk), 453
Fujimoto, M., & Tanahashi, Y. 1971a, PASJ, 23, 7
Fujimoto, M., & Tanahashi, Y. 1971b, PASJ, 23, 13
Fukui, Y., et al. 1999, PASJ, 51, 745
Hartmann, D., & Burton, W. B. 1997, Atlas of galactic neutral hydrogen (Cambridge: Cambridge University Press) CD-ROM
Haslam, C. G. T., Salter, C. J., Stoffel, H., & Wilson, W. E. 1982, A&AS, 47, 1
Heiles, C. 1996, ApJ, 462, 316
Honma, M., & Sofue, Y. 1997, PASJ, 49, 453
Ikuta, C., & Sofue, Y. 1997, PASJ, 49, 323
Imamura, K., & Sofue, Y. 1997, A&A, 319, 1
Kudoh, T., Matsumoto, R., & Shibata, K. 1998, ApJ, 508, 186
Kudoh, T., Matsumoto, R., & Shibata, K. 1999, Comp. Fluid Dyn. J., 8, 56
Martos, M., Allen, C, Franco, J., & Kurtz, S. 1999, ApJ, 526, L89
Matsumoto, R, Uchida, Y., Hirose, S., Shibata, K., Hayashi, M. R., Ferrari, A., Bodo, G., & Norman, C. 1996, ApJ, 461, 115
Mouschovias, T. Ch., & Paleologou, E. V. 1980, ApJ, 237, 877
Roberts, W. W. 1969, ApJ, 158, 123
Shibata, K., & Uchida, Y. 1986, PASJ, 38, 631
Shibata, K., & Uchida, Y. 1985, PASJ, 37, 31
Shibata, K., & Uchida, Y. 1987, PASJ, 39, 559
Smith, G. P. 1963, Bull. Astron. Inst. Netherlands, 17, 203
Sofue, Y. 1976, A&A, 48, 1
Sofue, Y. 1985, PASJ, 37, 507
Sofue, Y. 1994, ApJ, 431, L91
Sofue, Y. 2000, ApJ, 540, 224
Sofue, Y., & Tosa, M. 1974, A&A, 36, 237
Sofue, Y., & Vogler, A. 2001, A&A, 370, 53
Sofue, Y., Wakamatsu, K., & Malin, D. F. 1994, AJ, 108, 2102
Uchida, Y., & Shibata, K. 1985, PASJ, 37, 515
Wakker, B. P., & van Woerden, H. 1991, A&A, 250, 509